ISSN: 2454-9940

INTERNATIONAL JOURNAL OF APPLIED SCIENCE ENGINEERING AND MANAGEMENT

E-Mail :
editor.ijasem@gmail.com
editor@ijasem.org

www.ijasem.org

INTERNATIONAL JOURNAL OF APPLIED SCIENCE ENGINEERING AND MANAGEMENT

ISSN2454-9940

www.ijasem.org

Vol 9, Issue 1, 2014

EFFICIENT POWER MANAGEMENT: MULTIPORT BIDIRECTIONAL LLC RESONANT CONVERTER FOR GRID-TIED PHOTOVOLTAIC-BATTERYHYBRID SYSTEMS

[#1]V.M. Ramaapriya, Research scholar, Dept. of EEE, Bharath University, Chennai.
[#2]Dr. P. Chandrasekhar, professor, Dept. of EEE, Adams Engineering college, Paloncha.

ABSTRACT: In recent years, there has been a surge of interest in the study of distributed power generation facilities that include photovoltaic (PV) systems and energy storage for integration into the power grid. When using many energy sources at once, adding more DC-DC converters complicates the problem. This study presents a multiport bidirectional DC-DC LLC resonant converter for grid-linked applications that potentially address this issue. Furthermore, we created a zone-based controller approach that uses a modified maximum power point tracking (MMPPT) method based on the incremental conductance method. This is implemented to make it easier to manage the proposed system. When connecting to or disconnecting from the electric grid, this controller is recommended for controlling the voltage and flow of electricity. The converter in this study consists of a voltage source grid-tied inverter, an LLC resonant converter, and a bidirectional buck-boost converter. The voltage, battery, and PV are all capable of communicating with one another. Comprehensive simulation studies using MATLAB/Simulink have proved the functionality of the suggested architecture.

Keywords: Multiport converter, PV-battery hybrid system, Bidirectional LLC resonant converter, MPPT.

1. INTRODUCTION

Power distribution system power electronic converters and control systems build durable transmission networks. The outcome is smaller, stronger, and more efficient. One power converter regulates batteries, fuel cells, wind, and photovoltaics, which is new. The volumes have many converter topologies. Unidirectional and bidirectional converters exist. Numerous unidirectional converter studies exist. Despite its many benefits, it is not the best technique to reduce program size in isolated systems. When highly integrated energy sources and unidirectional converters merge, converters may increase. This increases system size and cost. Convertor power share control instability may reduce system efficiency.

So bidirectional converters work for devices with multiple energy sources. This architecture is used in V2G, battery storage, motor transmissions, and UPS. They work nicely with high-frequency SSAs. Power density, economy, and high-voltage connectors. Continuous developments allow more devices to connect to a converter. Therefore, multiport converter designs evolved. Green energy, battery storage, and loads were coupled via three-port half-bridge converters. A converter port power transmission diagram simplified it. An innovative three-port DC-DC converter with zero voltage switching was investigated for fuel cell and battery storage system integration. Controlled power flow, soft-switched, and maintained stability. CPUs have pros and cons. Three converters and wrapped transformers enhance system complexity, cost, and area.

To solve these problems, researchers created two-wound transformer multiport converters. New two-way DC-DC converters with isolated

terminals were shown. Supercapacitor and hybrid battery storage systems use it. The utility grid, load port, and battery storage were connected via a modified isolated half-bridge converter. Control sets resulted from converter mode tests. A modified half bridge converter connected an isolated output port to a battery store that delivered and received power. Tri-port full-bridge converters were made. The converter's construction and production were studied.

We seek a power converter design that reduces loss, increases efficiency, power density, and frequency, and uses renewable energy. Due to design requirements, more than hard-switching converters exist. LLC resonant converters and soft-switching improved. Green energy systems may benefit from high-frequency LLC resonant converters' high power densities across a wide input voltage range. Zero-voltage switching saves power.

Multiport resonant converters incorporating photovoltaics and battery storage have been shown. A half-bridge LLC resonant converter exists. This setup connects two sources to one PV and battery. A non-isolated resonant multiport switching capacitor stores and uses renewable energy. PWM and FFM controlled system output power and levels. Instead of the converter, a three-port LCL resonant converter fed power from PV and battery storage to the load. Another LLC design included a dual-energy vessel. Passive components make these designs expensive and big. Sharing input terminal power reduced switching. For multisource applications, bidirectional is superior since multiport systems cannot carry electricity from load to input ports.

The display's multiport LLC resonant converter powered all terminals. The three-winding transformer, semiconductor devices, inductors, and capacitors make the converter larger and more expensive. Both symmetric resonant tanks of a two-way LLC converter operate at the same frequency. We employed few resonant components to maximize power density. An auxiliary clamping switch with flying capacitors and a three-level resonant converter switched power both ways. Valve and battery additions may complicate and cost more. We propose a two-way power sharing converter with automatic output-to-input switching and an additional inductor. Converter efficiency and variable frequency transmission were limited by voltage gain ratio. Unlike LLC converters, a new architecture is efficient throughout a large voltage increase range. A buck-boost LLC converter can step-down in reverse and up in forward power flow using soft-switching.

Despite having two ports, these converters exceed study guidelines. For hybrid systems with battery storage, PV, and grid electricity, the converter needs three interfaces. Additionally, the battery adapter must be bidirectional. This converter uses two LLC resonant converters or a three-winding transformer. Some LLC resonant converter designs can increase power density and efficiency without a second or three-winding transformer, according to studies.

2. OVERVIEW OF TOPOLOGY

Figure 1 illustrates the converter's suggested configuration. The PV system, battery energy storage, and utility line are the system's three main components. The DC line Vdc is shared by both battery and PV energy storage. This bus can be regarded as either an input or an output, depending on the resonant converter's working mode. The battery energy storage is linked to the PV via a bidirectional buck-boost converter, resulting in the two terminals of the bidirectional converter at node A. The converter's second port is for utility infrastructure. It travels through a voltage source transformer. The high frequency

transformer allows the transmission of electricity between nodes A and B. As shown in Figure 1, the voltage, Vpv, of the PV system is the source of renewable energy.

The voltage in the battery is denoted by Vbat, the input capacitor by Cpv, and the bidirectional buck-boost converter's inductance as Lbat. This two-way converter is setup using switches Q1 and Q2. The input or output DC voltage of the LLC resonant converter can be thought of as Vdc or Vo, depending on the mode of operation. The DC transit capacitors at nodes A and B are designated as Cdc and Co, respectively. The resonant converter's bridges are made up of the switches P1, P2, P3, P4, S1, S2, S3, and S4. The magnetizing inductance of the high frequency transformer is Lm, whereas the resonant capacitance is Cr and the resonant inductance is Lr. Connecting all of the ports together allows for the creation of a multiport isolated bidirectional DC-DC converter. The three-phase voltage source inverter is comprised of switches G1–G6.

Proposed converter operation principle

Maximum power point monitoring (MPPT) is turned on to maximize the PV system's power output. Control the water flow in the battery energy storage device to achieve the MPPT. The three-phase voltage source inverter, which is connected to the grid, can transmit energy from the grid to the batteries or from the PV and batteries back to the grid. The power may come from the power line, the batteries, or the PV system. As a result, this converter arrangement can function in both forward and backward. Figure 2 shows four instances of each of the two kinds.

Forward Mode

When the converter operates in forward mode, power is transferred from node A to node B. This is the location of the three electricity-sharing zones. Figures 2a, b, and c depict these locations.

The PV system directly supports the quantity of electricity consumed by the grid and batteries in Zone I. The S1 through S4 switches on the bidirectional LLC converter and the Q1 switch on the bidirectional buck-boost are both inoperative in this zone, as shown in Fig. 3. As a result, it is clear that the battery storage is constantly being charged by the power supplied by the PV system; hence, it is categorized as a burden. In addition to transporting electricity from the PV system to the utility, this voltage source inverter serves other purposes. Furthermore, it follows the grid's power standard.

In Zone II, both the battery storage and the PV system send power to the grid. The S1 through S4 switches on the bidirectional LLC converter and the Q2 switch on the bidirectional buck-boost are both inactive in this zone, as shown in Figure 4. The battery storage device may now supply power to the grid.

The S1–S4 switches on the bidirectional LLC converter and the Q2 switch on the bidirectional buck boost are not activated in Zone-III, as shown in Fig. 5. As a result, the batteries serve as the sole source of electricity for the grid. In the majority of cases, the PV system fails to generate any power at night.

Reverse Mode

When electricity is transferred from node B to node A, the adapter works in reverse. In this stage of operation, only the grid and the battery energy storage system can share power, as shown in Figure 2(d). The battery storage device is a consumer in reverse mode of operation, as it is constantly charged by the grid. Switches P1 through P4 and Q2 are not operational, as shown in Figure 6, however switches S1 through S4 are.

INTERNATIONAL JOURNAL OF APPLIED SCIENCE ENGINEERING AND MANAGEMENT

ISSN2454-9940

www.ijasem.org

Vol 9, Issue 1, 2014

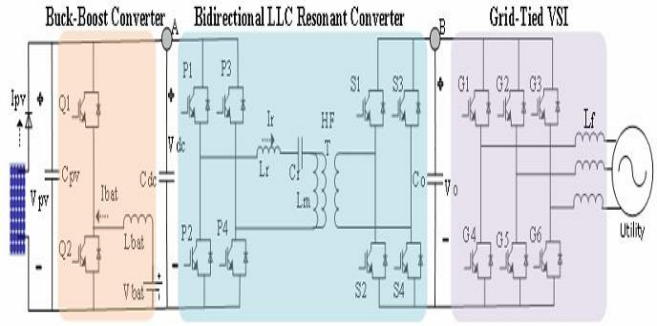

Fig. 1: The proposed multi-port resonant converter topology.

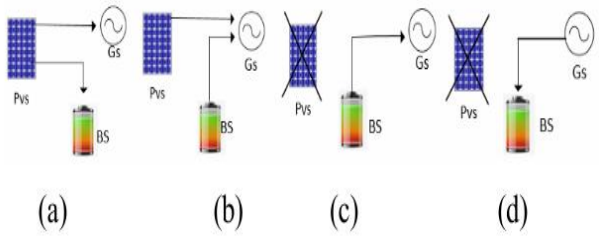

Fig. 2. Characterizing power flow in the PV, storage, and grid systems: I (b) II (c) Forward operation Zones Forward operations Zone-III (d) Reversed mode.

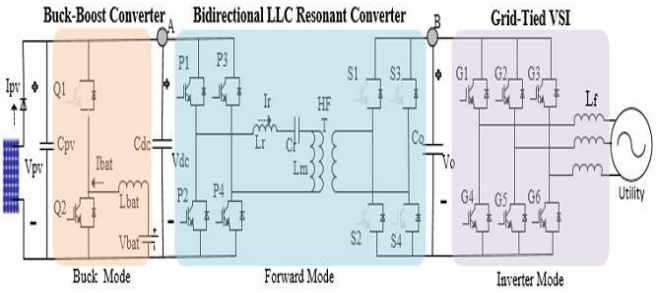

Fig. 3. Forward mode operation for Zone-I.

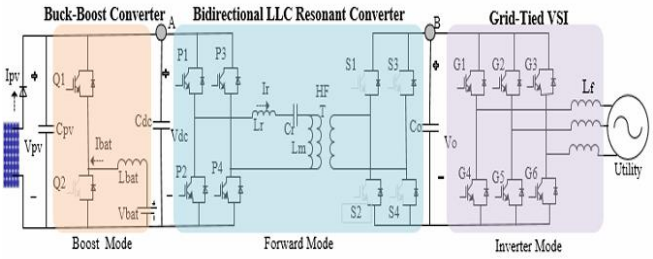

Fig. 4. Forward mode operation for Zone-II.

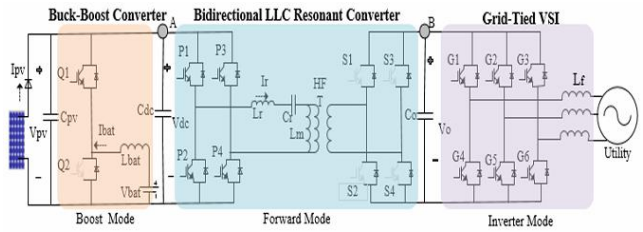

Fig. 5. Forward mode operation for Zone-III.

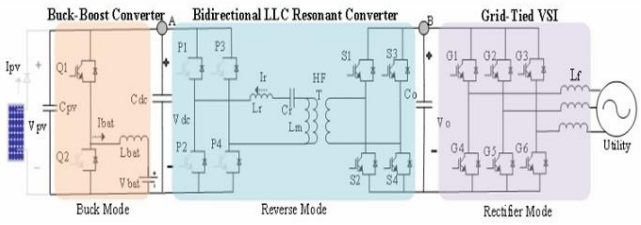

Fig. 6. Reverse mode operation.

3. CHARACTERISTICS OF DC VOLTAGE GAIN IN THE PROPOSED CONVERTER

There are two resonant frequencies in an LLC resonant converter. The resonant inductor Lr and resonant capacitor Cr determine the first resonance frequency. The second resonant frequency is determined by combining the magnetizing inductance Lm, the resonant inductor Lr, the resonant capacitor Cr, and the two transformer inductances. The initial resonance frequency is denoted by fr1, and the second by fr2.

$$f_{r1} = \frac{1}{2\pi\sqrt{L_r C_r}} \quad (1)$$

$$f_{r2} = \frac{1}{2\pi\sqrt{(L_r+L_m)C_r}} \quad (2)$$

Equations (3) and (4), along with the related circuit models presented in Fig. 7, can be utilized to theoretically determine the LLC resonant converter's DC gain.

$$K_{Forward} = \frac{aV_b}{V_a} = \frac{sL_m \,//\, R_o}{\frac{1}{sC_r} + sL_r + sL_m \,//\, R_o} \quad (3)$$

$$K_{backward} = \frac{aV_a}{V_b} = R_o + \frac{1}{sC_r} + sL_r + sL_m \quad (4)$$

The simplified DC gain values for equations (3) and (4) are calculated using the following quantities: m (the ratio of the sum of the primary and resonant inductances), Q (the ratio of the square root of the resonance inductor and

INTERNATIONAL JOURNAL OF APPLIED SCIENCE ENGINEERING AND MANAGEMENT

ISSN2454-9940

www.ijasem.org

Vol 9, Issue 1, 2014

capacitor to the effective resistance), Rac (the value of the reflected load resistance), Fx (the normalized frequency), and a (the transformer's turn ratio).

$$Q = \frac{\sqrt{\frac{L_r}{C_r}}}{R_{ac}} \quad (5)$$

$$R_{ac} = \left(\frac{8}{\pi^2}\right)(a^2 \cdot R_o) \quad (6)$$

$$m = \frac{L_r + L_m}{L_r} \quad (7)$$

$$F_x = \frac{f_s}{f_{r1}} \quad (8)$$

Because the converter is not connected to a specific load, the load resistance is assumed to vary. In (9), for example, power is transferred from node A to node B, but in (10), the opposite is true. Typically, the following figures show the load resistance in both forward and reverse operation phases:

$$R_o = \frac{V_o^2}{P_o} \quad (9)$$

$$R_o = \frac{V_{bus}^2}{P_{bat}} \quad (10)$$

The pattern examined in this research suggests that forward power transmission is the process of delivering power from node A to node B. When it is delivered from node B to node A, it is referred to as reverse power transfer. As a result, the first set of equations generated two gain values. Using these values, one can construct the next set of equations.

$$K(Q, m, F_x) = \frac{1}{\sqrt{\left[1+\frac{1}{m}\left(1-\frac{1}{F_x^2}\right)\right]^2 + \left(F_x - \frac{1}{F_x}\right)^2 \cdot Q^2}} \quad (11)$$

$$K(Q, m, F_x) = \sqrt{1 + \left(F_x - \frac{1}{F_x}\right)^2 \cdot Q^2} \quad (12)$$

To make the converter more user-friendly, the frequency of state transitions can be adjusted. Figure 8 depicts the suggested converter design's gain path for a variety of resistance values in both power modes.

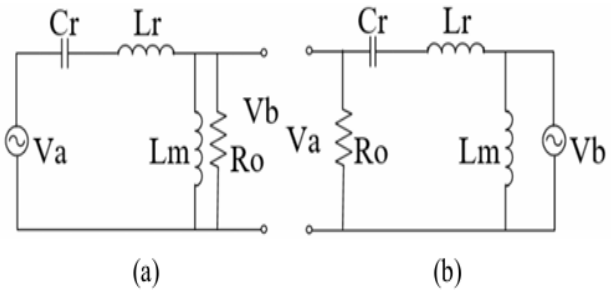

Fig.7. Circuit models that are equivalent to a bidirectional LLC resonant converter. (a) The use of the forward mode. (c) The use of the reverse mode

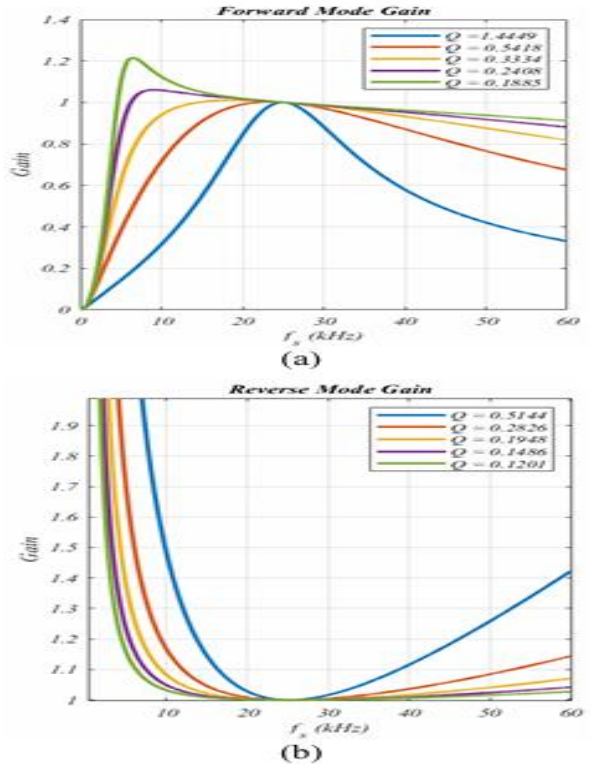

Fig. 8. DC gain of the two-way LLC converter for different Q values in the following modes: a) forward, b) reverse.

4. PROPOSED SYSTEM CONTROL TECHNIQUE

The control approach of this construction is designed to keep the converter stable in both forward and reverse phases. Figures 9 and 2 can be used to govern the situation. 1SOLTECH 1STH-350-WH Monocrystalline PW modules are used in this study. The PV system consists of four parallel strands. Each string consists of nineteen photovoltaic modules connected in series. Figure 9 shows the MPPT curve for this PV connection. Figure 2 depicts the control technique as follows:

Zone-I and -II

It is critical to maximise the power output of the PV in Zones I and II when transmitting power from node A to node B. This is why the PV's Maximum Power Point (MPP) was measured in order to calculate the battery's reference current using the MMPPT, a theory derived from the well-known Incremental Conductance (IC) method.

When the intensity of solar radiation exceeds a predefined threshold, the MMPPT activates and starts regulating the battery's reference current. As a result, the PV system's operating condition is used to estimate the charging and discharging current. The battery's reference current decreases when the working point is on the right side of the MPP. If you want a lower reference current, you can change the battery storage's operating mode to increase or decrease its power output. Equation (15) demonstrates this situation.

When the system working point is on the left side of the MPP, the MMPPT increases the battery's reference current. This is different from the right side. This suggests that the charging capacity may be increased or reduced. Equation (14) illustrates this method. The MMPPT keeps the battery's reference current constant when the working point is at the MPP. Equation (13) depicts this action point.

$$\text{At the MPP} \quad \frac{\Delta I}{\Delta V} = -\frac{I}{V} \Rightarrow Ibat^*(k) = Ibat^*(k-1) \tag{13}$$

$$\text{The left side} \quad \frac{\Delta I}{\Delta V} > -\frac{I}{V} \Rightarrow Ibat^*(k) = Ibat^*(k-1) - \Delta I \tag{14}$$

$$\text{The right side} \quad \frac{\Delta I}{\Delta V} < -\frac{I}{V} \Rightarrow Ibat^*(k) = Ibat^*(k-1) + \Delta I \tag{15}$$

Figure 10 illustrates the approved MMPPT method. The efficiency of this control mechanism is seen in Fig. 11. The trajectory of solar radiation is likewise visible, as is the battery's proportionate reference current. These were discovered via the MMPPT method. As previously indicated, the MMPPT measures the battery's power and status (charging or draining).

Zone-III

PV electricity is either unavailable or below the set point for operation in Zone III. The mode identification algorithm disables the MPPT method and regulates battery storage using the voltage regulation approach, as shown in Figure 13. It is clear from Figure 13(a). At this point, a PI regulator is purchased to maintain the proper DC bus voltage. The PI regulator establishes the battery's reference current in order to keep the DC bus voltage stable.

The variable switching frequency approach, in conjunction with the control strategies described for Zones I, II, and III, must be used to manage the DC voltage, or Vo, of the full bridge LLC resonant converter in order to transfer power from node A to node B. In this arrangement, the controller sets up the secondary switches P1, P2, P3, and P4.

Reverse Mode

The voltage source inverter is in correction mode, and the electricity is supplied by the utility. In these cases, the mode detection approach calculates the battery's reference current, which is set by a separate PI controller that regulates the battery's voltage. In reverse mode, rather than forward mode, the full bridge LLC resonant

INTERNATIONAL JOURNAL OF APPLIED SCIENCE ENGINEERING AND MANAGEMENT

ISSN2454-9940

www.ijasem.org

Vol 9, Issue 1, 2014

converter is set to maintain a constant DC bus voltage (Vdc) at node A. Figure 13(b) shows how the switches S1, S2, S3, and S4 on the transformer's secondary side change when the allow signal is sent. The switches P1, P2, P3, and P4 are all inactive.

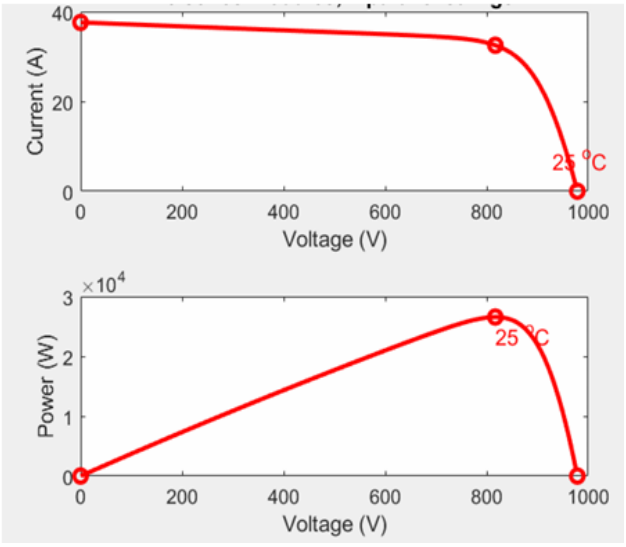

Fig. 9. The I-V and P-V curves

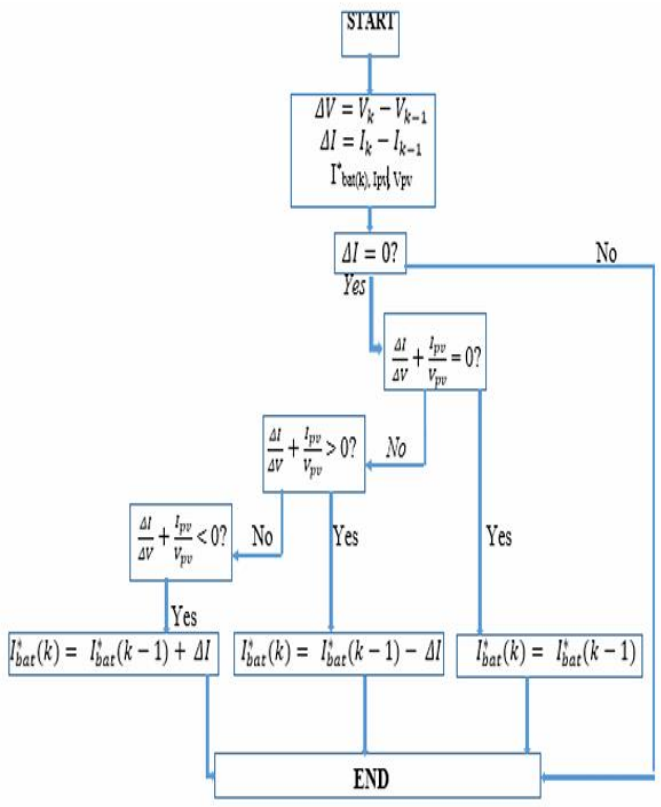

Fig. 10. Flowchart of the MMPPT controller

Finally, the cascaded controller regulates the operation of the LLC resonant converter, as shown in Figure 13(b). In the recommended control scenario, the outer voltage control loop serves as the current reference for the inside current loop. A low-pass filter with a cut-off frequency of fr1 prevents the resonance current from flowing. The voltage source inverter control system is set up to receive an active power reference from a higher-level CPU as power is delivered from node A to node B. The voltage source transformer is designed to have a power factor of one. As a result, the reactive power is constant in both modes of operation. In contrast, the active portion of the current is transmitted from node B to node A by a PI controller that is set to keep the DC voltage Vo at the desired level. The three-phase currents delivered to the grid are regulated using the synchronous reference frame current management approach, as shown in Figure 13(c).

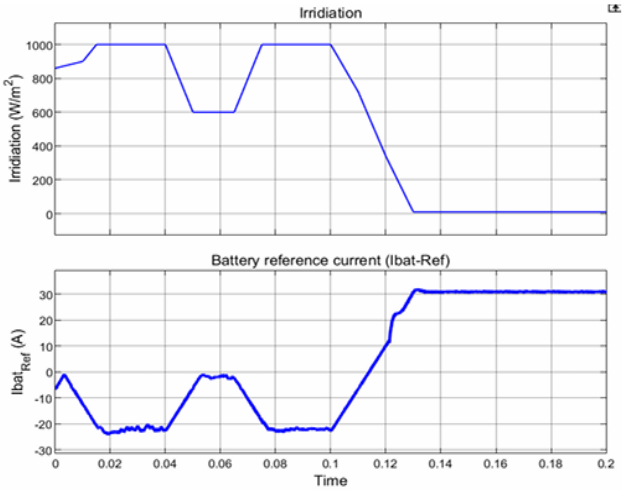

Fig. 11. MMPPT controller performance

INTERNATIONAL JOURNAL OF APPLIED SCIENCE ENGINEERING AND MANAGEMENT

ISSN2454-9940

www.ijasem.org

Vol 9, Issue 1, 2014

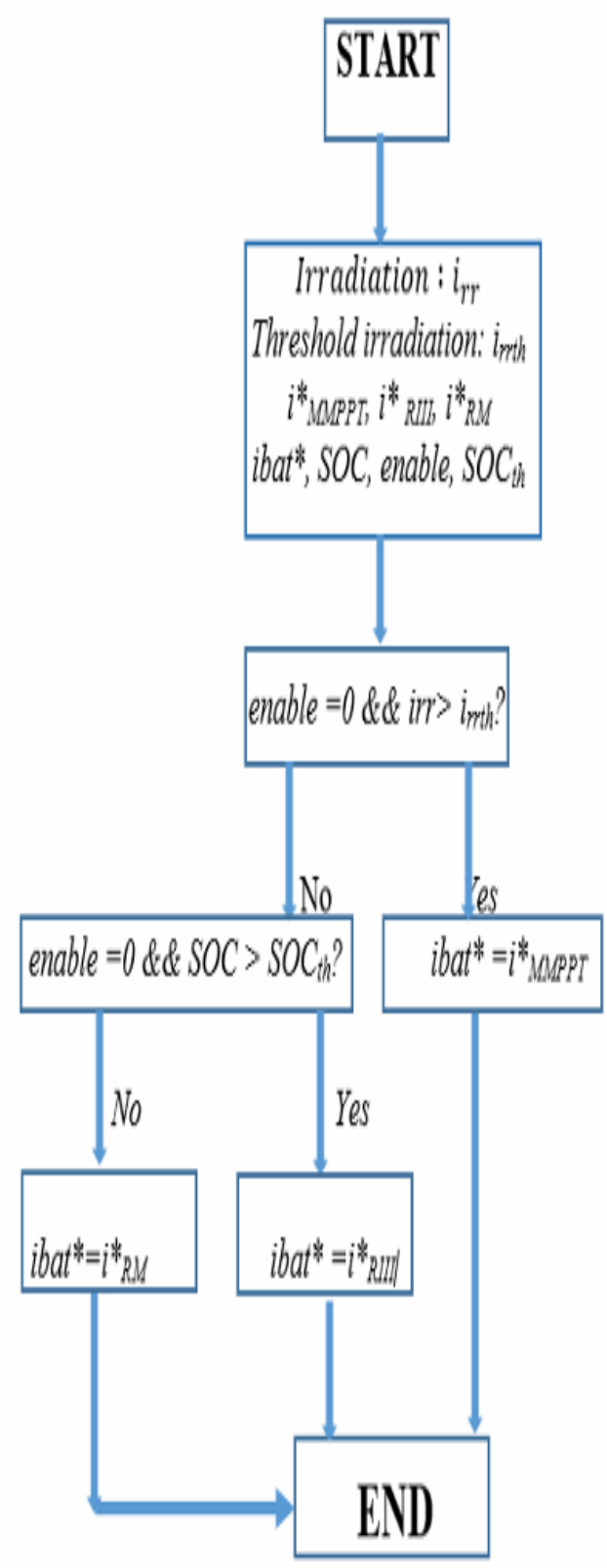

Fig. 12. Mode detector algorithm

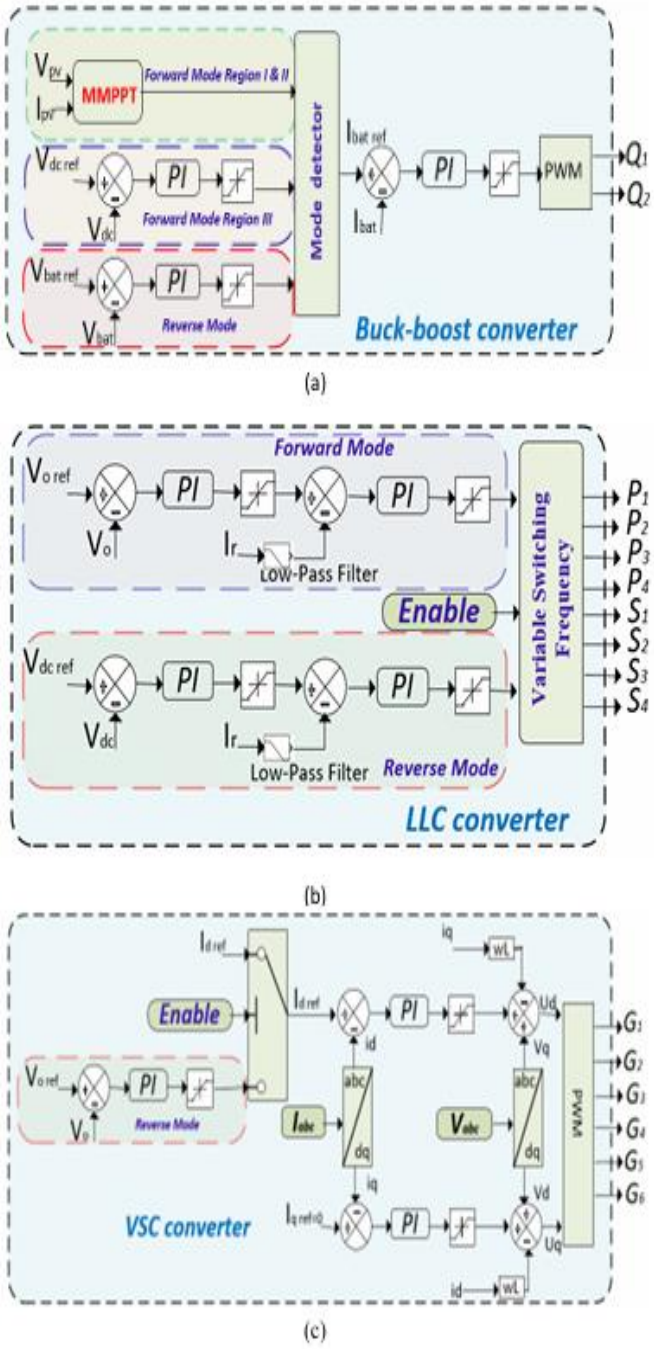

Fig. 13. Control of the proposed topology a) The MMPPT and battery charge/discharge controller b) The output voltage control (c) The voltage source inverter control

5. SIMULATION RESULTS

A bidirectional multiport LLC resonant converter and MMPPT control mechanism monitor a power

grid-connected battery-photovoltaic system's MPP. Our MATLAB/Simulink simulations tested the design and control method in real life. System components include a bidirectional buck boost converter, LLC resonant converter, and grid-connected voltage source inverter. Recommended system parameters are in Table 1.

The voltage source converter's active power is seen by the d-axis current holding at 20 A when power is transferred from node A to B. The q-axis current constant 0 A represents reactive power. People know Zone I's PV system generates more power than it exports. The energy storage unit holds surplus PV electricity. Utility cannot get enough PV electricity in Zone II. Machine stability comes from energy storage. Zone III has no PV power. The grid runs on energy storage alone. Infrastructure transports electricity from node B to A to power the energy storage unit.

Figure 14 shows operational mode and three-zone battery, PV, and grid voltage, current, and power waveforms. The grid's mean is power, current its root-mean-square. Different curves.

After briefly oscillating around the MPP, the MMPPT controls the battery's reference current for the bidirectional buck boost converter's current regulator (Figure 14). PV regulates battery power to optimum power. Node B's DC voltage and the voltage source inverter's DC bus are maintained by the bidirectional LLC resonant converter. Transformers power three-phase AC.

PV power and irradiation drop at t=0.1s. PV system MPP is maintained via MMPPT battery standard management. The MMPPT is turned off and battery current adjusted to maintain voltage when PV power drops below a threshold. Zone-III is battery-powered. The bidirectional LLC resonant converter maintains node B voltage. Zones I, II, and III operate on batteries. Node B becomes a battery by supplying grid electricity to Node A in reverse. Fig. 14's converter structure switches modes smoothly and performs effectively in all conditions.

Figure 15 displays three-phase grid currents and voltages. Before t=0.2s, voltage source transformer transmits PV/battery power to grid. At t=0–0.2, a higher-level CPU gives 20A to the voltage source inverter. This inverter changes from grid to battery power at t=0.2s. Under these conditions, PI regulators set reference current. The regulator maintains 800V for the inverter DC bus. Since the switchover, grid electricity has changed little.

In practice, maximum current values are constrained to protect hardware. Maximum study power is 30 amps. Maximum battery charging is 20A. Figure 15 shows that the inverter is effective in both cases since it responds quickly and stays constant. Inverter THD is 1.35%, rectifier 1.27%. All three-phase currents are sinusoidal.

Battery voltage, current, and SOC% are given in Figure 16. Set SOC 30%. Reverse and Zone I charge batteries. Zones II and III movies. The intended layout for each activity zone is shown here. Figure 17 shows both phases' LLC resonant converter main, secondary, and leakage currents.

Table1. System Parameters

Parameters	Value
Resonant inductor, L_r	10μH
Magnetizing inductor, L_m	250μH
Resonant capacitor, C_r	4μF
Switching frequency (LLC resonant converter)	20-60kHz
Switching frequency (Buck-Boost Converter)	30 kHz
Switching frequency (VSI)	10 kHz
Output voltage, V_o	800V
Battery voltage, V_{bat}	460-540V
Grid voltage (phase to neutral, rms) and frequency, V_g, f_g	230V/50Hz
Inductance (Buck-Boost Converter), L_{bat}	0.7mH
VSI output filter, L_{inv}	2mH

INTERNATIONAL JOURNAL OF APPLIED SCIENCE ENGINEERING AND MANAGEMENT

ISSN2454-9940

www.ijasem.org

Vol 9, Issue 1, 2014

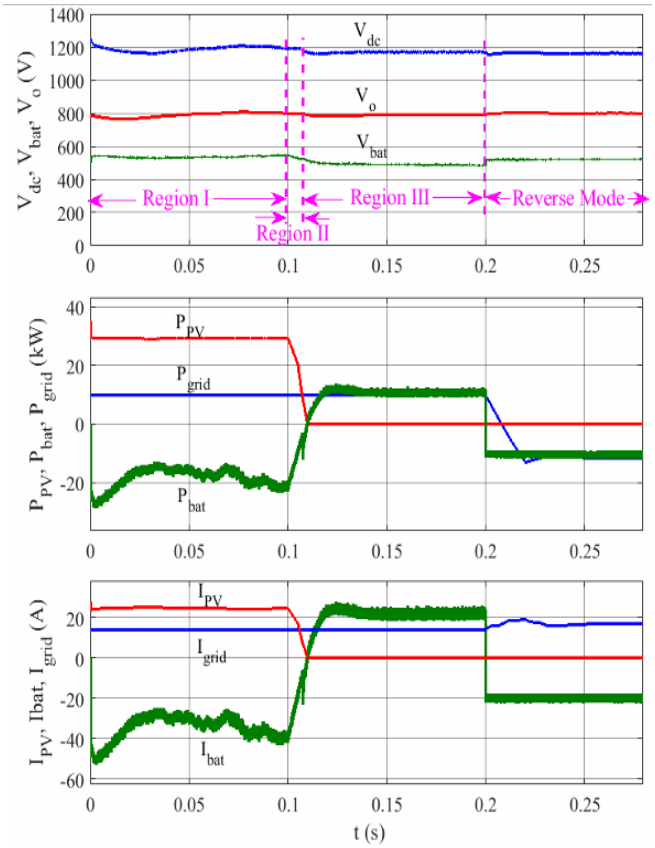

Fig. 14. Proposed system operation waveforms for all three regions and reverse mode.

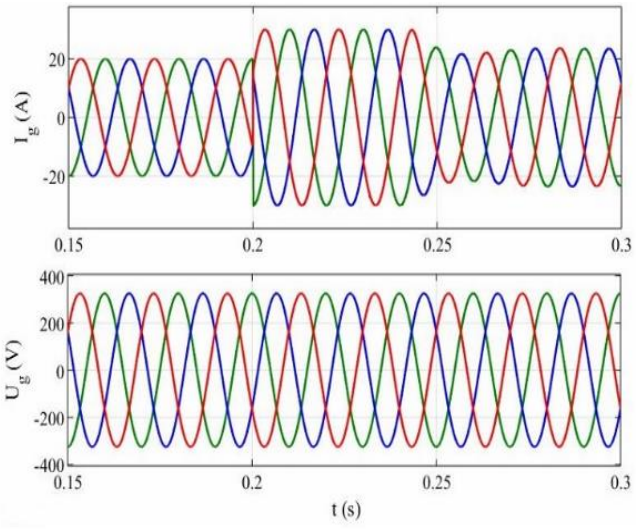

Fig. 15. Three-phase grid currents and voltages.

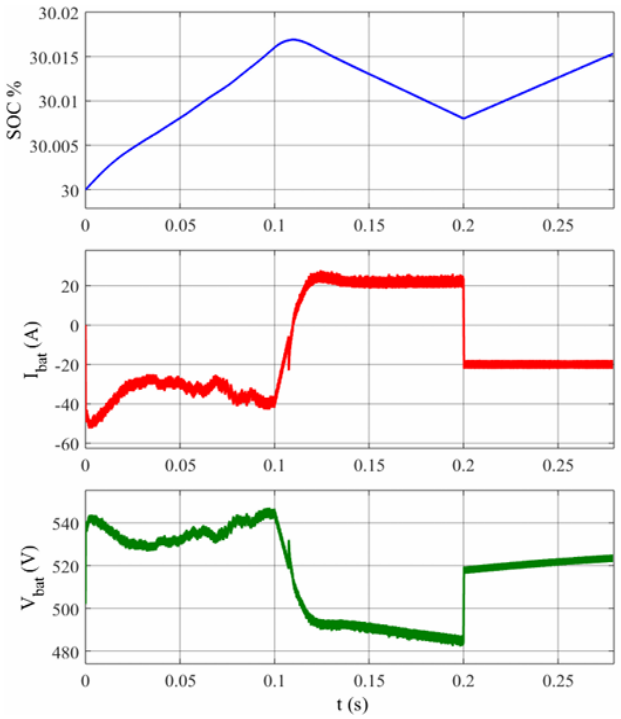

Fig. 16. Battery voltage, current, and charge stats.

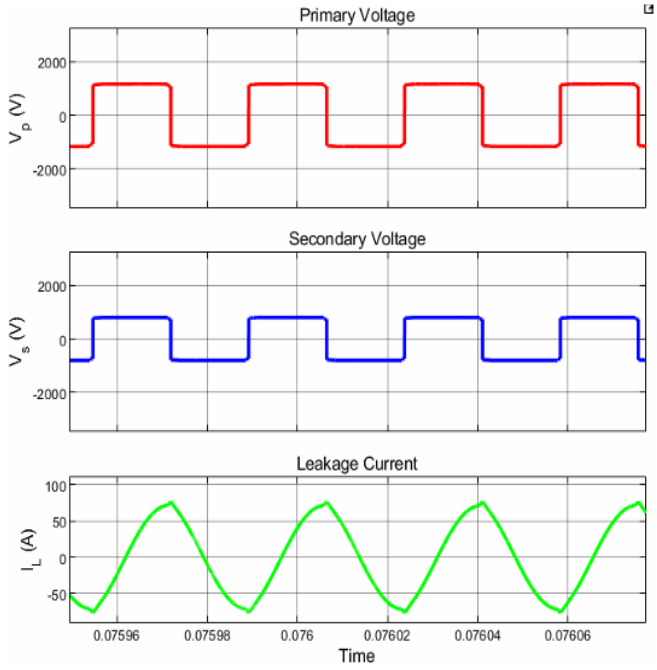

(a)

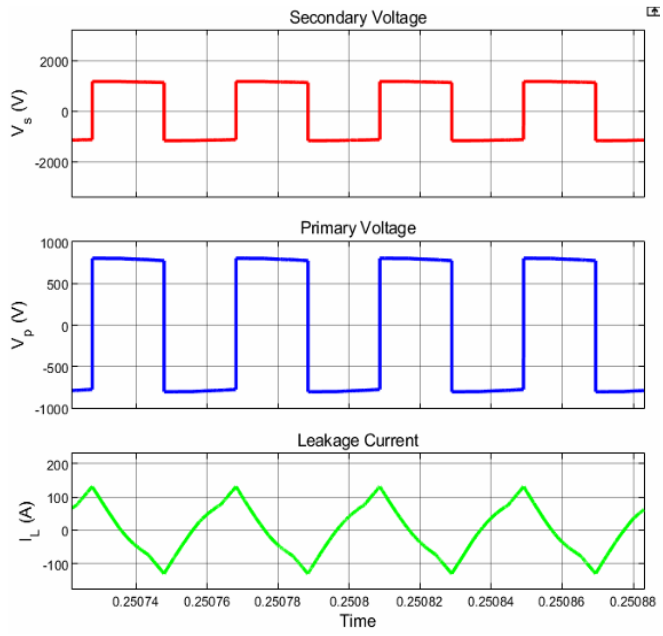

(b)

Fig. 17. Primary and secondary voltages and leakage currents of the converter (a) Forward mode (b) Reverse Mode

6. CONCLUSION

This study describes a multiport bidirectional LLC resonant converter that works with grid-connected PV and storage systems. The bidirectional buck boost converter connects the battery to the same node. Next, the LLC resonant converter interface at node A is connected directly to the PV system. Furthermore, the three-phase voltage source transformer aids in the transfer of power between nodes A and B and the three-phase AC grid. A control mechanism is established to ensure the stability of the proposed system's voltages and currents in all operational modes, as well as to manage the flow of power between ports. It has been proved that the proposed structure works in all three zones and both modes of operation. Furthermore, power transmission across all ports is accurate and consistent, independent of mode of operation. It is advised that two sources be combined into a single transformer to protect the grid against galvanic current. This improves the power density and efficiency.

REFERENCES

1. H. Tao, A. Kotsopoulos, J. L. Duarte and M. A. M. Hendrix, "Family of multiport bidirectional DC-DC converters," IEE Proceedings - Electric Power Applications, vol. 153, no. 3, pp. 451-458, 1 May 2006
2. T. Labella, W. Yu, J.-S. Lai, M. Senesky, and D. Anderson, “A bidirectional-switch-based wide-input range high-efficiency isolated resonant converter for photovoltaic applications,” IEEE Trans. Power Electron., vol. 29, no. 7, pp. 3473–3484, 2014.
3. M.-H. Ryu, H.-S. Kim, J.-H. Kim, J.-W. Baek, and J.-H. Jung, “Test bed implementation of 380V DC distribution system using isolated bidirectional power converters,” 2013 IEEE Energy Conversion Congr. and Exposition, 2013.
4. H. Tao, A. Kotsopoulos, J. L. Duarte, and M. A. M. Hendrix, “Transformer-coupled multiport ZVS bidirectional DC–DC converter with wide input range,” IEEE Transactions on Power Electronics, vol. 23, no. 2, pp. 771–781, 2008.
5. Z. Qian, O. Abdel-Rahman and I. Batarseh, "An Integrated Four-Port DC/DC Converter for Renewable Energy Applications," IEEE Transactions on Power Electronics, vol. 25, no. 7, pp. 1877-1887, July 2010.
6. Phattanasak, Matheepot, Roghayeh Gavagsaz-Ghoachani, Jean Philippe Martin, Babak Nahid-Mobarakeh, Serge Pierfederici, and Bernard Davat. “Control of a Hybrid Energy Source Comprising a Fuel Cell and Two Storage Devices Using Isolated Three-Port Bidirectional DC–DC Converters.” IEEE Transactions on Industry Applications 51, no. 1 (2015): 491–97.

7. Z. Ding, C. Yang, Z. Zhang, C. Wang, and S. Xie, “A novel soft switching multiport bidirectional DC–DC converter for hybrid energy storage system,” IEEE Transactions on Power Electronics, vol. 29, no. 4, pp. 1595–1609, 2014.
8. Al-Atrash, Hussam, Feng Tian, and Issa Batarseh. “Tri-Modal Half Bridge Converter Topology for Three-Port Interface.” IEEE Transactions on Power Electronics 22, no. 1 (2007): 341–45.
9. Qian, Zhijun, Osama Abdel-Rahman, and Issa Batarseh. “An Integrated Four-Port DC/DC Converter for Renewable Energy Applications.” IEEE Transactions on Power Electronics 25, no. 7 (2010): 1877–87.
10. Wu, Hongfei, Kai Sun, Runruo Chen, Haibing Hu, and Yan Xing. “Full Bridge Three-Port Converters With Wide Input Voltage Range for Renewable Power Systems.” IEEE Transactions on Power Electronics 27, no. 9 (2012): 3965–74.
11. H. Hu, X. Fang, F. Chen, Z. J. Shen and I. Batarseh, "A Modified HighEfficiency LLC Converter With Two Transformers for Wide InputVoltage Range Applications," in IEEE Transactions on Power Electronics, vol. 28, no. 4, pp. 1946-1960, April 2013.
12. X. Sun, X. Li, Y. Shen, B. Wang and X. Guo, "Dual-Bridge LLC Resonant Converter With Fixed-Frequency PWM Control for Wide Input Applications," IEEE Transactions on Power Electronics, vol. 32, no. 1, pp. 69-80, Jan. 2017
13. Y. Wei, N. Altin, Q. Luo and A. Nasiri, "A High Efficiency, Decoupled On-board Battery Charger with Magnetic Control", 2018 7th International Conference on Renewable Energy Research and Applications (ICRERA), Paris, 2018, pp. 920-925.
14. S. Milad Tayebi, X. Chen, A. Bhattacharjee and I. Batarseh, "Design and Implementation of a Dual-Input LLC Converter for PV-Battery Applications," 2018 IEEE Energy Conversion Congress and Exposition (ECCE), Portland, OR, 2018, pp. 5934-5940.
15. M. Uno and K. Sugiyama, “Switched capacitor converter-based multiport converter integrating bidirectional PWM and series-resonant converters for standalone photovoltaic systems”, IEEE Transactions on Power Electronics, pp. 1–1, 2018.
16. J. Zeng, W. Qiao, and L. Qu, “An isolated three-port bidirectional DCDC converter for photovoltaic systems with energy storage,” 2013 IEEE Industry Applications Society Annual Meeting, 2013.
17. T. Jiang, Q. Lin, J. Zhang and Y. Wang, "A novel ZVS and ZCS threeport LLC resonant converter for renewable energy systems," 2014 IEEE Energy Conversion Congress and Exposition (ECCE), Pittsburgh, PA, 2014, pp. 2296-2302.
18. K. Tomas-Manez, Z. Zhang and Z. Ouyang, "Multi-port isolated LLC resonant converter for distributed energy generation with energy storage," 2017 IEEE Energy Conversion Congress and Exposition (ECCE), Cincinnati, OH, 2017, pp. 2219-2226.
19. H. Krishnaswami and N. Mohan, "Three-Port Series-Resonant DC–DC Converter to Interface Renewable Energy Sources With Bidirectional Load and Energy Storage Ports," IEEE Transactions on Power Electronics, vol. 24, no. 10, pp. 2289-2297, Oct. 2009.
20. E.-S. Kim, J.-H. Park, J.-S. Joo, S.-M. Lee, K. Kim, and Y.-S. Kong, “Bidirectional DC-DC converter using secondary LLC resonant tank”, 2015 IEEE Appl. Power Electron. Conf. and Exposition (APEC), 2015.